El Niño, La Niña, and the Nonlinearity of Their Teleconnections

MARTIN P. HOERLING

CIRES/CDC, University of Colorado, Boulder, Colorado

ARUN KUMAR

NOAA/NCEP, Washington, D.C.

MIN ZHONG

CIRES/CDC, University of Colorado, Boulder, Colorado

ABSTRACT

The paradigm of an atmospheric system varying linearly with respect to extreme phases of the El Niño–Southern Oscillation is questioned. It is argued that the global response to tropical Pacific sea surface temperature forcing will be inherently nonlinear. A physical basis for this intrinsic nonlinearity is the thermodynamic control on deep convection.

Climate statistics for warm and cold events of the tropical Pacific are analyzed separately for the northern winter periods during 1950–96. Composite analysis of 500-mb heights reveal planetary-scale teleconnection patterns, as noted in earlier studies. A new result is the evidence for an appreciable 35° longitude phase shift between the warm and cold event circulation composites, and the two wave trains appear to have different tropical origins. A large nonlinear component in North American surface climate anomalies is also found, which is consistent with such a phase shift in teleconnections. In the Tropics, rainfall anomalies also show evidence of nonlinear behavior. The maximum rain anomalies along the equator are located east of the date line during warm events, but west of the date line during cold events. The interpretation of this behavior is complicated, however, by the fact that composite warm event SST anomalies are not the exact inverse of their cold event counterparts.

Idealized atmospheric general circulation model (AGCM) experiments are performed in order to test the question of whether the observed nonlinearity is an intrinsic property of the atmospheric system. The model is forced with a composite SST anomaly that undergoes a realistic seasonally varying ENSO life cycle, as described by E. Rasmusson and T. Carpenter. Both positive and negative phases of the SST anomaly are used, and a 40-member ensemble of warm and cold event model simulations is conducted. A nonlinear climate response in the AGCM is found that closely resembles the observed composites, including a shift in the equatorial positions of the maxmium rain responses and a phase shift of teleconnection patterns in the upper troposphere. Barotropic model experiments indicate that the inherent nonlinearity in the tropical rain response may itself be responsible for the phase shift in the extratropical teleconnection patterns.

1. Introduction

The prevailing view of the global atmospheric climate signal associated with El Niño–Southern Oscillation is of a linear response, with anomalies during the El Niño (warm) phase being the inverse of those during the La Niña (cold) phase. Evidence in support of this linear view emerges primarily from tropical analyses, however. For example, Bradley et al. (1987) show that the temperature and precipitation response over tropical land masses tends toward two inverse states with respect to the Southern Oscillation (SO), a result confirmed by

Ropelewski and Halpert (1989). Such results have been used to justify the practice of portraying global climate anomalies associated with the SO as the difference between warm and cold events (e.g., van Loon and Rogers 1981; Pan and Oort 1983; Kiladis and Diaz 1989). Implicit in this practice is the assumption that the linear part of the climate response dominates, although the nonlinear component of the global response has not been explored.

That even the tropical response may not be linear for equal and opposite SST anomalies is implicit in the thermodynamic control on deep convection. Oceanic regions of climatologically active convection depend on the underlying value of sea surface temperature to a good approximation (e.g., Gadgil et al. 1984), and little convective activity takes place over SST values colder

---

Corresponding author address: Dr. Martin P. Hoerling, CIRES/CDC, University of Colorado, Boulder, CO 80309.
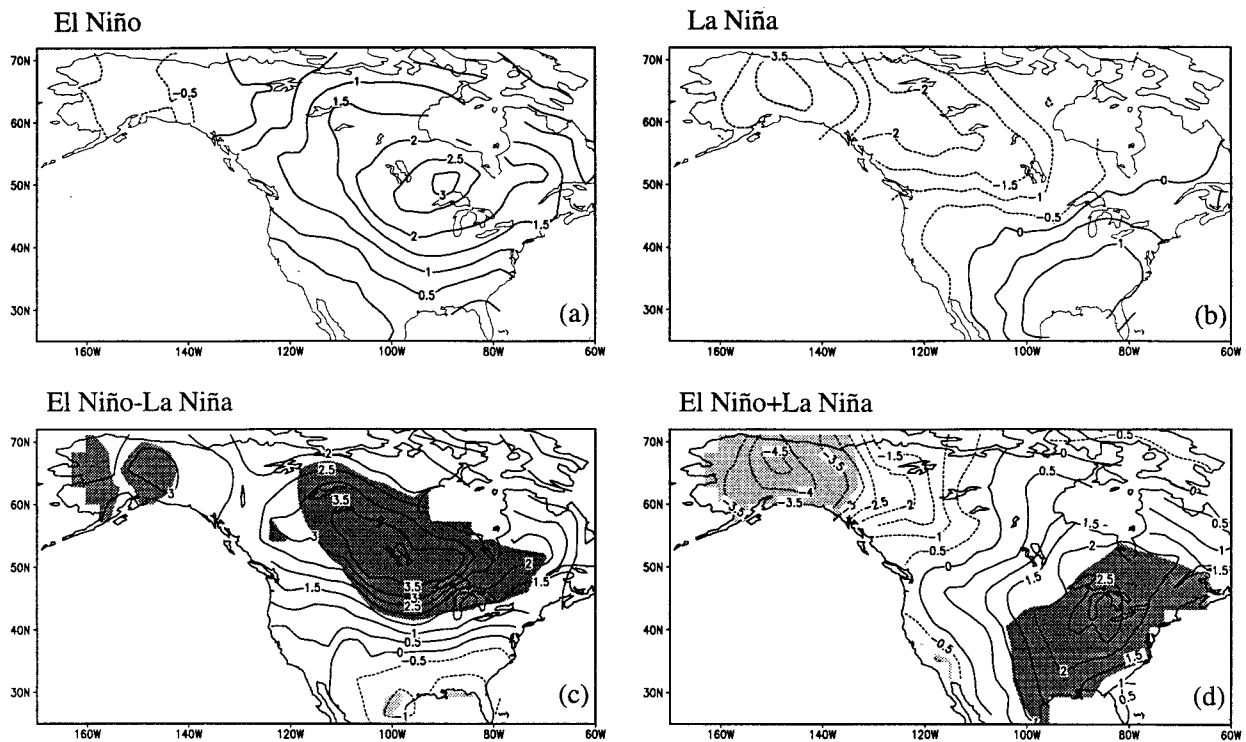
FIG. 1. Composites of the seasonally averaged DJF observed surface temperature anomalies for (a) El Niño and (b) La Niña states of the tropical Pacific sea surface temperatures. See Table 1 (section 2) for the years included in the composites. (c) Linear component of the surface temperature anomalies as estimated by the difference (a) minus (b). (d) Nonlinear component of the surface temperature anomalies, as estimated by the sum (a) plus (b). Contour interval is 0.5°C. Dark (light) shading indicates local statistical significance of positive (negative) values at the 95% confidence level.

than 27°C. Due to the zonal asymmetries of the climatological SSTs, even small deviations of the sea surface temperature from its climatological value can excite large rainfall deviations on the periphery of the west Pacific warm pool region, whereas positive anomalies of appreciable amplitude are required to induce convection within the east equatorial Pacific cold tongue. On the other hand, negative SST anomalies in the cold tongue region have no further effect on the normally dry conditions, leading to appreciable nonlinearity between the effects of El Niño and La Niña on tropical rainfall. Thus, an important characteristic of the climate system is that the maximum interannual variability in rainfall over the equatorial Pacific is shifted several thousand kilometers west of the maximum interannual SST variability (Deser and Wallace 1990).

The question thus becomes whether such an inherent nonlinear relationship between SST and deep convection can also lead to inherent differences in extratropical responses to opposite phases of tropical SST forcing. The few empirical studies that have examined the differences in mean anomalies for extremes of the SO have provided some evidence for nonlinearity in the signal over North America. Dole et al. (1994) find extreme winter mean temperature events over the contiguous United States to be associated primarily with warm events. Sittel (1994) finds the marginal probability of extreme rainfall and temperature over the southeastern United States to be a highly nonlinear function of the SO's phase. Since 1946, for example, the warm event enhanced rainfall signal has been much larger than the cold event suppressed signal in the southeastern United States.

As further evidence for nonlinearity in the North American climate sensitivity, Figs. 1a and 1b present composite wintertime [December–February (DJF)] surface temperature anomalies for El Niño and La Niña, respectively. Each composite is an average of nine events during 1950–96, the procedures for selection being described in section 2. The maximum warm temperature anomaly during El Niño is located over south-central Canada, but this resides at the zero temperature anomaly line of the La Niña composite, and the two maps are nearly in quadrature. A difference of the two maps estimates the linear component of the ENSO response with respect to tropical central Pacific SST anomalies (Fig. 1c) and is consistent with earlier studies that feature a zonally oriented pattern dividing the continent along 40°N. A summation of the two maps estimates the nonlinear component (Fig. 1d). This features a meridionally oriented pattern dividing the continent along 110°W.

Most intriguing is the equality of the implied linear and nonlinear components of the North American temperature anomalies in Fig. 1. One may thus argue that much is forfeited by analysis methods based on assumptions of linearity and much is to be gained by treating the North American climate response to warm and cold events separately.

Is the nonlinearity seen in Fig. 1 an intrinsic property of the atmospheric system when forced with equal and opposite tropical SST anomalies? The empirical results alone are insufficient evidence for such nonlinearity, due to several factors. First, due to sampling, the patterns in Fig. 1 undoubtedly represent some blend of an SST-forced signal and climate noise that is independent of the state of the SSTs. Interpretation of observations is further complicated by the fact that the equatorial Pacific SST anomalies are themselves not linear functions of the SO (Philander 1990). Thus, for example, some of the differences between Figs. 1a and 1b may also originate from different SST life cycles during warm and cold events.

Such caveats notwithstanding, the aforementioned inherently nonlinear SST–rainfall relationship in the Tropics offers a plausible mechanism that could induce nonlinearity in the extratropical response. It remains to be determined whether appreciable differences in tropical rainfall that are relevant for tropical–extratropical interactions indeed exist.

There are additional internal atmospheric sources that can lead to an asymmetric extratropical response for equal and opposite tropical SST anomalies. These arise due to the complicated chain through which the tropical SSTs influence extratropical climate. Included in these are (i) changes in the mean flow through which energy from tropical sources propagates into higher latitudes (e.g., Blade and Hartmann 1995) and (ii) the sensitivity of storm tracks to different background flows (e.g., Hoerling and Ting 1994; Branstator 1995). Apart from the possible asymmetries in the extratropical responses forced by inherent differences in the tropical heating, the way in which these additional dynamic sources may contribute to asymmetric teleconnection patterns also remains an open question.

This study explores a physical and dynamic basis for the emerging observational suggestions of asymmetries in the North American climate response to extreme phases of the Southern Oscillation. We begin in section 3 with a planetary-scale analysis of the linear and nonlinear anomalies in sea level pressure, sea surface temperature, and upper-level circulation patterns that are associated with warm and cold events separately. Rainfall proxies are also analyzed for the nonlinearity of the local tropical response. The question is then posed as to whether the observed nonlinearities are an intrinsic property of the atmospheric system alone, namely in the absence of any further nonlinearity arising from non-symmetric evolution of warm and cold SST events themselves.

A suite of idealized atmospheric general circulation model (AGCM) experiments is thus performed in order to investigate this question. As described in section 2, these experiments are designed to overcome several limitations posed by observations. First, both El Niño and La Niña SST anomalies used as lower-boundary conditions in the AGCM are precisely symmetric and evolve through realistic 16-month ENSO-like life cycles. Second, a large ensemble (40) of such integrations is performed for both warm and cold states in order to ensure unambiguous detection of the SST-forced signals. The AGCM results in section 4 also show evidence for nonlinearity, and simple dynamic model calculations are presented in section 5 in order to explore the mechanisms involved. Section 6 provides a summary and concluding comments.

2. Datasets and methods

a. Analysis of observations

Global sea surface temperatures are analyzed for the winter seasons during 1950–96[1] using a combination of two datasets. A new monthly near-global SST dataset is used for the 1950–81 period. This uses eigenvector reconstruction to estimate SST values at ocean points on a 2° latitude–longitude grid and is described in Smith et al. (1996). For the period since 1982, the combination of in situ measurements and satellite observations is adequate to resolve the global SST field. The monthly mean SSTs for the period 1982–96 are available on a 1° latitude–longitude grid, and the analysis is based on the optimum interpolation method described in Reynolds and Smith (1994). This recent dataset is interpolated to a 2° grid and joined with the historical data.

The selection of warm and cold events is based on an analysis of area-averaged SSTs for 160°E–120°W, 5°N–5°S, an area encompassing the entire Niño-4 region and the western portion of the Niño-3 index region. Although not sampling the longitudes of maximum interannual SST variability, the importance of this region lies in the large local sensitivity of deep convection and the resultant forcing of global atmospheric teleconnections. An index of the standardized SST anomalies for this region is formed, and the nine winters having the largest positive index values and the nine winters having the largest negative index values are selected. These correspond roughly to the one standard deviation or greater SST departures of the 1950–96 record, are consistent with those identified in other empirical studies, and are listed in Table 1 (e.g., Kiladis and Diaz 1989).

Composites are used to examine the Northern Hemisphere climate patterns associated with warm and cold events separately. Monthly mean land-surface temperature data, based on the station network, are available

---

[1] The indicated year refers to January of the winter season.

TABLE 1. List of warm and cold event years (1950–96) used in the composite analysis.

Warm events								
1958	1966	1969	1973	1983	1987	1988	1992	1995
Cold events								
1950	1951	1955	1956	1965	1971	1974	1976	1989

for 1950–95. Monthly mean analyses of sea level pressure for the region between 15° and 90°N are also available on a 5° latitude–longitude grid. Trenberth and Paolino (1980) address quality issues of the sea level pressure data, and we use the subset of that data that covers the 1950–95 period. The National Center for Environmental Prediction's (NCEP) monthly mean 500-mb height analyses covering the period 1950–95 are used to diagnose the midtropospheric stationary wave patterns. The data cover the region 20°–90°N and have been interpolated to a regular 2.5° grid.

Since one purpose of this study is to investigate the nonlinear part of the climate response associated with the SO, the composite anomalies for the variables listed above are computed relative to a climatology of years that excludes the 18 winters of extreme SST states. Thus, the base period consists of 29 yr having "near-normal" tropical Pacific wintertime SSTs.

A somewhat different procedure is required for the analysis of tropical rainfall, due to a lack of spatial coverage from in situ measurements over oceanic regions. We thus rely on remote sensing estimates of that rainfall using polar orbiting satellite measurements of outgoing longwave radiation (OLR). The advantage of this dataset over other satellite products is its 23-yr availability from March 1974 to the present, and we use the globally complete OLR dataset described in Liebmann and Smith (1996). In order to form warm and cold event OLR composites, another standardized SST anomaly time series is generated covering only the 1974–96 period (not shown) and a selection of the five warmest (1983, 1987, 1988, 1992, 1995) and the five coldest (1975, 1976, 1984, 1985, 1989) SST events in this period is made. The strong controlling effect of the SSTs on local tropical rainfall should permit meaningful interpretation of these composites based on smaller samples. It should be noted that these composites are not based on the same selection of years as used for the circulation variables, based on our longer data record.

b. Atmospheric general circulation model experiments

Idealized SST anomaly experiments are performed using the atmospheric component of NCEP's coupled ocean–atmosphere forecast system. This model, including its physical parameterizations, is identical to the one described in Kumar et al. (1996) and has T40 spectral resolution with 18 unequally spaced sigma levels. Deep convection is parameterized by a Kuo scheme, and the

details of its implementation are given in the appendix of Kumar et al. (1996)

A "composite" El Niño based on the average of the five periods 1957–58, 1965–66, 1972–73, 1987–88, and 1991–92 is constructed. These cases were selected due to their overall similarity in evolution through the annual cycle. The first three cases are those included in the Rasmusson and Carpenter (1982) composite, and the evolution of our composite SST anomalies from the early months of the inital year of warming (year 0) to the decay phase in the middle of year +1 is very similar to that shown in their study.

The composite El Niño anomaly is added to the climatological SST for each month from February of year 0 through May of year +1. The climatology of each month is the 1982–94 average, and the anomaly is added only for the tropical Pacific basin within 20°N–20°S. This total SST then evolves daily as a boundary condition within a 16-month seasonal cycle integration of the AGCM.

An ensemble of 40 simulations is performed in which each integration, begun from different atmospheric initial conditions, experiences the same evolution of warm SST boundary conditions. A parallel set of 40 simulations is performed in which the SST anomaly is reversed in sign, yielding cold SST boundary conditions. The atmospheric initial conditions used to seed these anomaly runs are extracted from a 40-yr control integration that uses repeating annual cycle SSTs based on the 1982–94 average.

c. Barotropic model

A linear barotropic stationary wave model is used to interpret the AGCM's response to El Niño and La Niña SST forcing. The model equation can be written as

$$\frac{\partial \zeta'}{\partial t} + \overline{\mathbf{v}}_\psi \cdot \nabla \zeta' + \mathbf{v}'_\psi \cdot \nabla (\bar{\zeta} + f) = S' + D', \quad (1)$$

where $\mathbf{v}_\psi$ and $\mathbf{v}_\chi$ are rotational and irrotational components of the velocity, ζ is the relative vorticity, overbars represent climatological means, and primes refer to seasonal anomalies. The forcing associated with divergence is expressed as a source S' (Held and Kang 1987; Sardeshmukh and Hoskins 1988), given by

$$S' = -\nabla \cdot [\mathbf{v}'_\chi (\bar{\zeta} + f)] - \nabla \cdot (\overline{\mathbf{v}_\chi} \zeta'), \quad (2)$$

which includes both the vortex-tube stretching effect and the advection of vorticity by the divergent flow. The effects of dissipation are represented by D', according to

$$D' = -\kappa \zeta' + \nu \nabla^4 \zeta', \quad (3)$$

where κ is a drag coefficient equal to $(7 \text{ days})^{-1}$, as in our earlier studies with this model (e.g., Hoerling et al. 1992, 1993), and the biharmonic diffusion $\nu = 2 \times 10^{16}$ m⁴ s⁻¹. We spectrally transform (1) in the horizontal at rhomboidal wavenumber 15, and steady solutions are

El Niño

La Niña

(a)

(b)

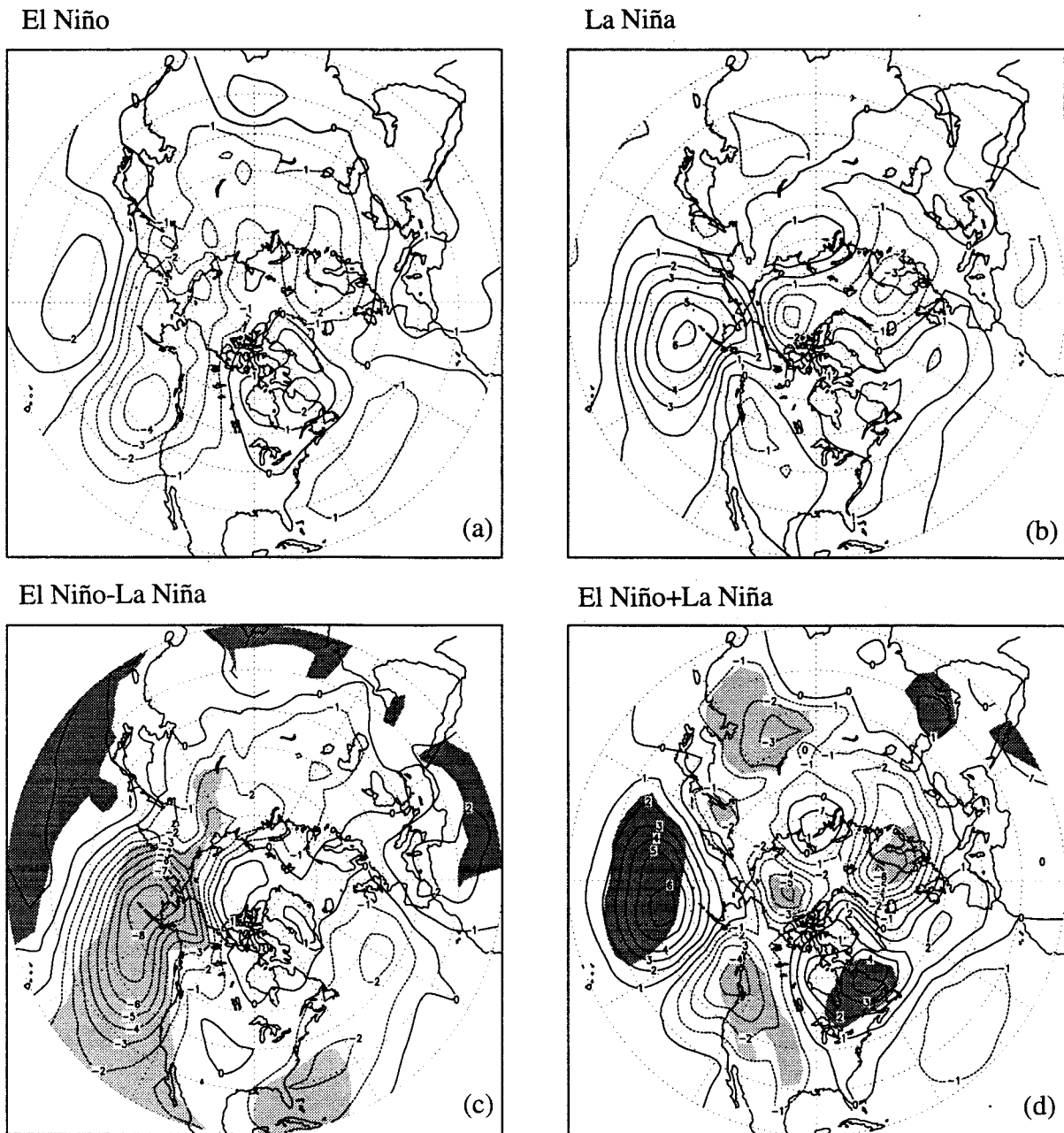El Niño-La Niña

El Niño+La Niña

(c)

(d)

FIG. 2. Same as in Fig. 1 except for the observed mean sea level pressure. Contour interval is 1 mb. Polar stereographic projection extends to 20°N.

sought (i.e., omitting the first left-hand side term) using the matrix inversion method of Ting and Held (1990).

The basic-state flow used in (1) is the AGCM's wintertime wavy 300-mb climatology, derived from the control run using climatological SSTs, whereas the forcing associated with divergence is derived from the AGCM anomaly runs for El Niño and La Niña SST states. The divergence anomalies are those located at the level of maximum outflow from tropical deep convection, which resides near the 200-mb level in the AGCM.

Our experiments explore the extratropical stationary wave adjustment to the AGCM's tropical divergence anomalies for El Niño and La Nina conditions. To the extent that the AGCM possesses a nonlinear tropical convective response to the imposed equal but opposite SST forcing, the barotropic model experiments assess the dynamic significance of this for the extratropical response.

There are uncertainties in the one-level barotropic model calculations, as discussed in Held et al. (1989)

El Niño
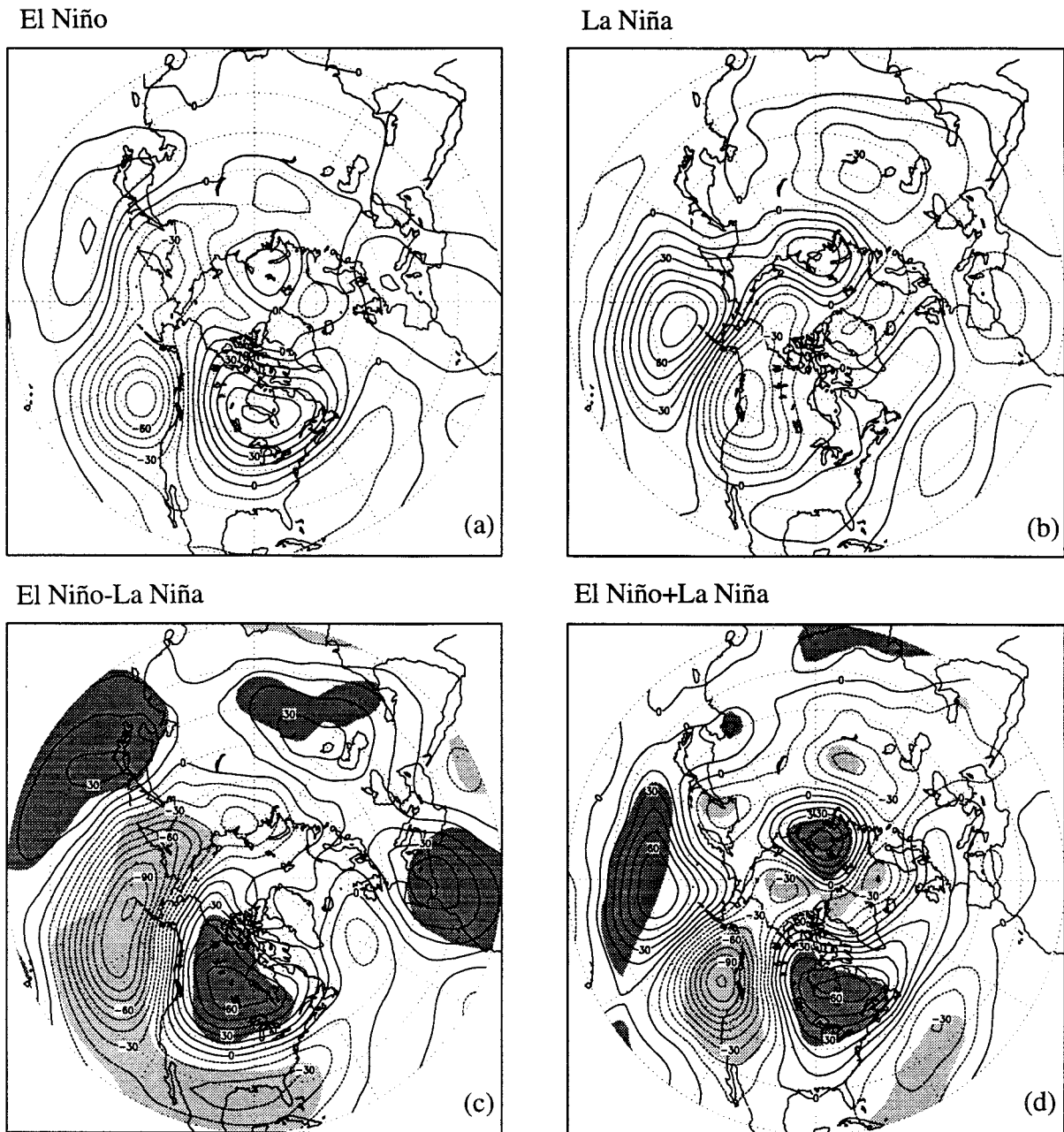
La Niña

El Niño-La Niña

El Niño+La Niña

FIG. 3. Same as in Fig. 1 except for the observed eddy 500-mb heights. Eddy refers to the departure of the height from its zonal mean value and indicates the stationary wave behavior. Contour interval is 10 m. Polar stereographic projection extends to 20°N.

and Held and Kang (1987). One issue involves the equivalent barotropic level for which (1) applies and the sensitivity of results to choices of that level. We have performed calculations at several levels ranging from 400 to 150 mb and find at least qualitative consistency of our main results for such a range of levels. Ting (1996) suggests that 350 mb may be an equivalent barotropic level for wintertime states when (1) is linearized about a zonally symmetric circulation. The equivalent barotropic level of a wavy base state, on the other hand,

is not well known and, undoubtedly, will be a function of location. The sensitivity of solutions to realistic choices of κ was also explored by using values ranging from $(5 \text{ days})^{-1}$ to $(14 \text{ days})^{-1}$. The forced solutions are found not to change their spatial phases, although amplitudes of the extratropical response increase significantly for weaker drags. A 7-day damping used herein appears consistent with estimates of the appropriate value of the damping at the equivalent barotropic level (e.g., Borges and Sardeshmukh 1995).
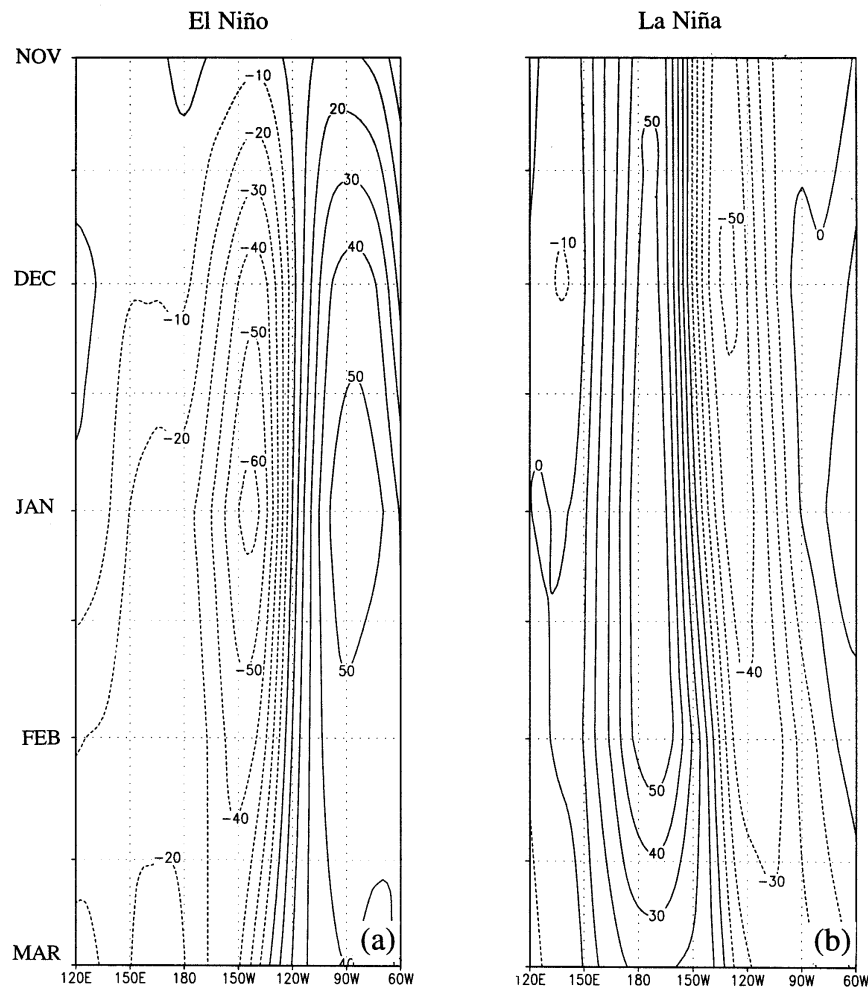
El Niño   La Niña

FIG. 4. Time–longitude sections of observed eddy 500-mb height anomalies composited with respect to (a) El Niño and (b) La Niña SST states. The heights are averages for the 45°–60°N latitude band, and the cross sections sample the Pacific–North American sector. Time varies from November of year 0 (top) to March of year +1 (bottom) of the composite SST event. The contours are smoothed using a 1–2–1 temporal filter. Contour interval is 10 m, and negative values are dashed.

3. Observed teleconnection patterns during El Niño and La Niña

Figure 2 presents the composite analysis of sea level pressure for the same selection of cases as used to construct the surface temperature composite in Fig. 1. Over the North Pacific, the couplet structure of the El Niño anomalies is consistent with an Aleutian low center shifted toward the U.S. west coast. In contrast, a monopole La Niña anomaly pattern indicates weakening of the Aleutian low's central pressure but little phase shift. Over North America, both composites have the same sign distribution of anomalies, and here the estimated linear component of the surface pressure response (Fig. 2c) is much weaker than its nonlinear counterpart (Fig. 2d).

Circulation anomalies at the 500-mb level largely

mirror those at sea level, revealing the well-known equivalent barotropic structure of the extratropical response (Fig. 3). Over the Pacific–North American (PNA) region, the El Niño composite has centers of action that project strongly on the Tropical–Northern Hemisphere (TNH) teleconnection mode of Barnston and Livezey (1987). In contrast, the La Niña anomalies are nearly in quadrature, and its principal centers of action project instead on the PNA teleconnection mode. Consistent with this is the result that the estimated linear (Fig. 3c) and nonlinear (Fig. 3d) components of the composite anomalies are comparable, as was the case for land-surface temperature and sea level pressure.

Nonlinearity in the midlatitude teleconnections associated with the extreme phases of the SO is largely due to a phase shift of the stationary wave anomalies.

El Niño

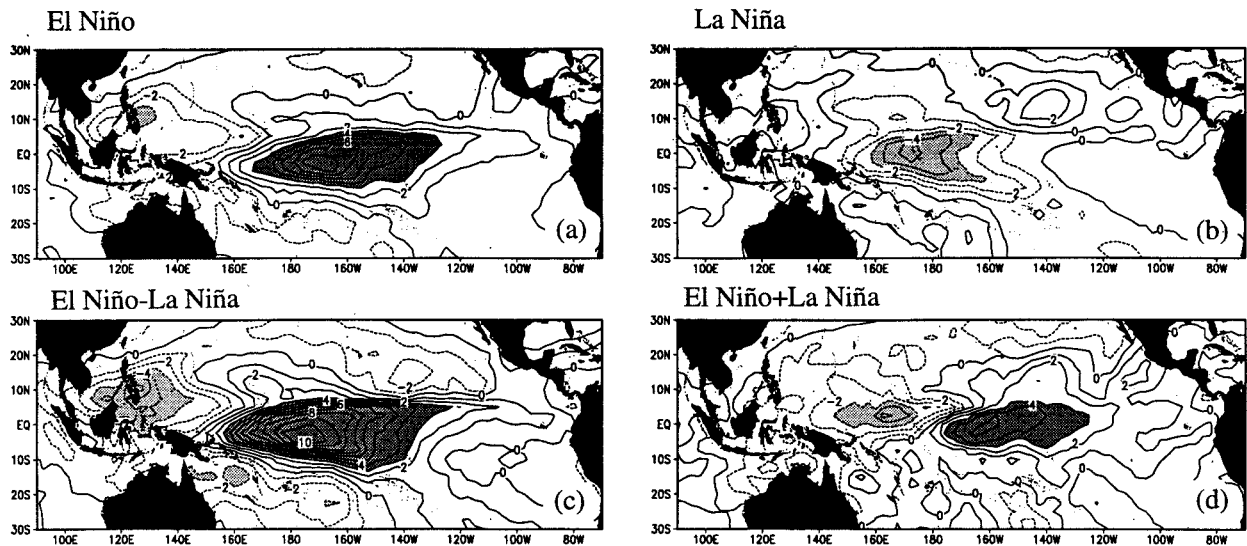La Niña

El Niño−La Niña

El Niño+La Niña

FIG. 5. Same as Fig. 1 except for rainfall anomalies. Rainfall estimates are derived from analysis of outgoing longwave radiation data for 1974–96, and conversion to rainfall units is based on the Arkin and Meisner (1984) empirical regression formula. Contour interval is 1 mm day^{-1}. Positive (negative) rainfall anomalies greater (less) than 3 mm day^{-1} are shaded dark (light). Mercator projection displays the tropical Pacific region 30°N–30°S.

Thus, the spatial correlation between El Niño and La Niña 500-mb stationary wave anomalies over the region 20°–70°N, 180°–60°W is only −0.2, but increases to −0.9 for a 35° eastward shift of the La Niña pattern. This phase shift is a consistent feature of the month-to-month midlatitude circulation anomalies for warm and cold events, as shown in Fig. 4. The longitude–time section depicts the height anomalies averaged between 45° and 60°N for longitudes of the Pacific–North American sector from November of year 0 to March of year +1. It is evident that the cold event centers of action are consistently west of their warm event counterparts, although their amplitudes are nearly identical. There are other features in the Hovmoeller that appear to distinguish the midlatitude circulation evolution during warm and cold events. For example, the cold event anomalies acquire maximum amplitude earlier in the annual cycle than their warm event counterparts. Note also that the cold event wave train shifts progressively eastward with time, and the phase difference between warm and cold event wave trains is largest in late fall and smallest in early spring.

A zero-order explanation for the phase shift in extratropical teleconnection responses to extremes of the SO is the differences in tropical diabatic forcing itself. Estimates of the rainfall anomalies during warm and cold events suggest that even the equatorial rainfall response in the vicinity of the strong SST forcing is a nonlinear function of that forcing. The center of enhanced deep convection lies east of the date line during El Niño, and positive rainfall anomalies extend along the equator to the South American coast (Fig. 5a). In contrast, the center of suppressed deep convection during La Niña (Fig. 5b) lies west of the date line, and

negative rainfall anomalies extend only to 140°W. The lack of a cold event rainfall signal farther east is consistent with the fact that the negative SST anomalies exert no further effect on the normally arid conditions within the core of the climatological cold tongue.

The linear component of the equatorial rainfall anomalies (Fig. 5c) consists of the well-known dipole pattern with out of phase centers located at the date line and 120°E. The date line anomaly is the stronger of the pair and is centered slightly south of the equator, whereas the anomaly of the opposite sign over the west Pacific is centered at 10°N.

The nonlinear component of the equatorial rainfall anomalies (Fig. 5d) also consists of a dipole pattern, although both centers have comparable amplitudes and their maxima are both equatorially centered. This component resembles, to a considerable degree, the rainfall anomaly pattern during the warm phase of the Southern Oscillation itself (Fig. 5a), and the amplitudes of this nonlinear component are comparable to that observed during a composite warm event. One main difference between Figs. 5a and 5d is the eastward shift and reduced half-wavelength of anomalies in the latter.

It is tempting to attribute the results in Fig. 5d to an inherently nonlinear relationship between SSTs and deep convection. Indeed, the observed difference between composite El Niño and La Niña rainfall patterns is physically consistent with the fact that positive SST anomalies can initiate deep convection within the core of the east Pacific cold tongue, whereas negative SST anomalies will have their largest effect on the periphery of the west Pacific warm pool region. There a reduction of the climatological SSTs to values below 27°C can greatly reduce deep convection.
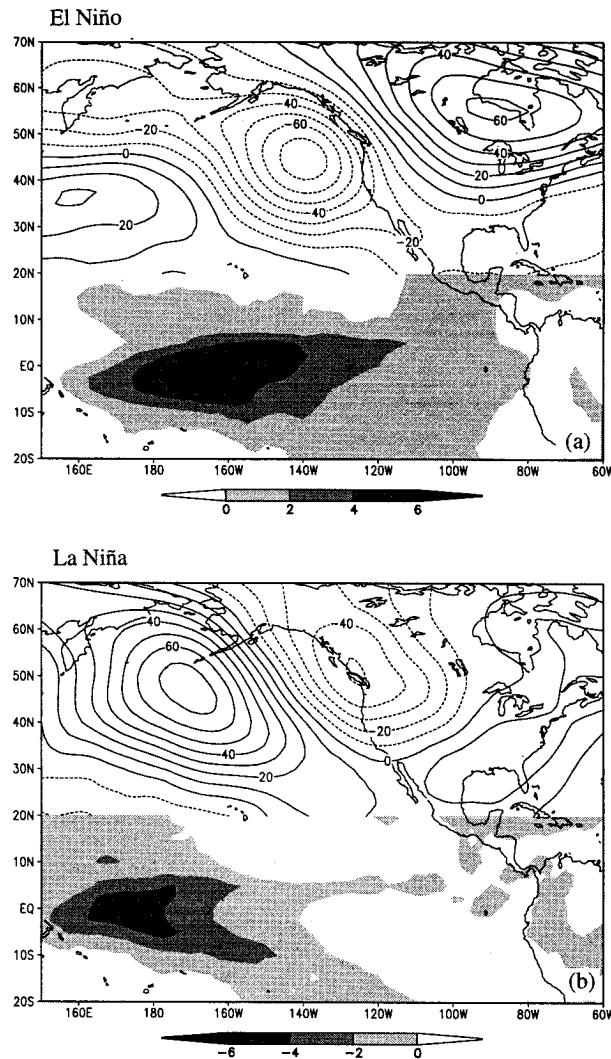
FIG. 6. The observed seasonally averaged DJF 500-mb eddy height and precipitation anomalies composited with respect to (a) El Niño and (b) La Niña SST states. Heights are shown only poleward of 20°N, and contours are drawn every 10 m. Precipitation is shown only equatorward of 20°N, and the various gray shades are drawn for 2 mm day^{-1} intervals.

Thus, it is enticing to speculate whether the phase shift between El Niño and La Niña equatorial rain anomalies may account for the phase shift of extratropical stationary wave anomalies evident in Fig. 3. Figures 6a and 6b combine the rainfall and circulaton anomalies for the El Niño and La Niña composites, respectively. One gets the impression that the two wave trains may have different tropical source regions, with the eastward phase shift of the El Niño pattern consistent with the eastward-shifted convection.

Complicating the interpretation of the observations, however, is the fact that the sea surface temperature anomalies themselves are not linear inverse functions of the Southern Oscillation. Larger SST anomalies during the mature phase winter season are observed in the

Niño-3 region during warm events (Fig. 7a) than during cold events (Fig. 7b). On the other hand, the cold event composite tends to have larger SST anomalies at this time of year within the Niño-4 region. The linear component of the tropical SST anomalies (Fig. 7c) is certainly much larger than the nonlinear component (Fig. 7d). However, which component of the nonlinearity in tropical rainfall is related to differences between warm and cold event SST forcing, and how much may arise even if such forcing were perfectly symmetric, remains an open question. It is within the latter scenario that one can assess the inherent nonlinearity of the tropical atmospheric response, a behavior that might account for the phase shift in extratropical teleconnection patterns.

The indication that the SSTs do not tend toward two inverse states with respect to the SO is intriguing. Whether this has a basis in ocean dynamics and is an indication of nonlinearity in the coupled atmosphere–ocean system or is perhaps merely a sampling artifact is a question beyond the scope of this study.

4. Sensitivity of an AGCM to El Niño and La Niña

We consider an idealized climate system in which the tropical SST anomalies associated with El Niño and La Niña undergo identical evolutions, but with reversed phase. As described in section 2, the composite SST anomaly is based on a selection of warm event years and closely follows that of Rasmusson and Carpenter (1982). As in their composite, SST anomalies are largest in the eastern Pacific during spring of year 0, shift into the central Pacific by fall of year 0, and return to near-normal values by the following spring of year +1. It is becoming evident that the SST life cycle of individual events can deviate appreciably from such a composite, but our interest here is to examine the linearity of the atmosphere's response to some realistic depiction of an ENSO SST life cycle. An analysis of the inter–El Niño SST variations and their possible significance for teleconnection patterns appears in Kumar and Hoerling (1997).

As for the observations, we focus on the AGCM's response during the northern winter season of year +1, at which time the composite SST anomaly acquires peak amplitude in the central Pacific. The spatial pattern of the wintertime SST anomaly used as a lower boundary forcing in the AGCM is very similar to that shown in Fig. 7a.

Equatorial Pacific rainfall responses to El Niño and La Niña are shown in Figs. 8a and 8b, respectively. These bear a strong similarity to the OLR estimates of observed rainfall, including the displacement of positive (negative) anomalies east (west) of the date line during El Niño (La Niña) and a larger maximum rainfall anomaly during the Southern Oscillation's warm phase. The resultant nonlinear component of the AGCM's rainfall response (Fig. 8d) consists of a dipole pattern having
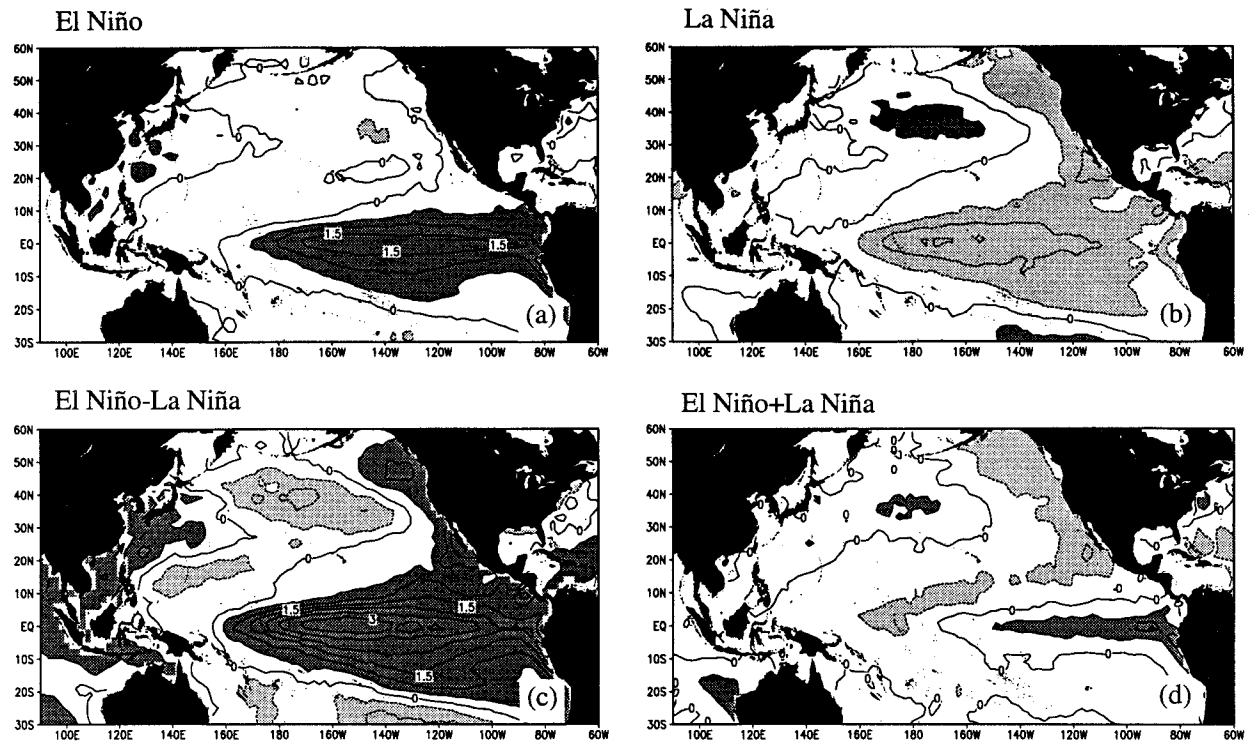
El Niño

La Niña

El Niño-La Niña

El Niño+La Niña

FIG. 7. Same as Fig. 1 except for sea surface temperatures. Contour interval is 0.5°C. Positive (negative) SST anomalies greater (less) than 0.5°C are shaded dark (light). Mercator projection displays the Pacific region 60°N–30°S.

equatorially centered enhanced rainfall east of the date line and suppressed rainfall west of the date line.

Given the strict linearity of the SST forcing in the designed AGCM experiments, the nonlinear component of the tropical rainfall response is unequivocally due to nonlinearity in the SST–deep convection relationship. Furthermore, the agreement between modeled and observed nonlinear equatorial rain responses suggests that
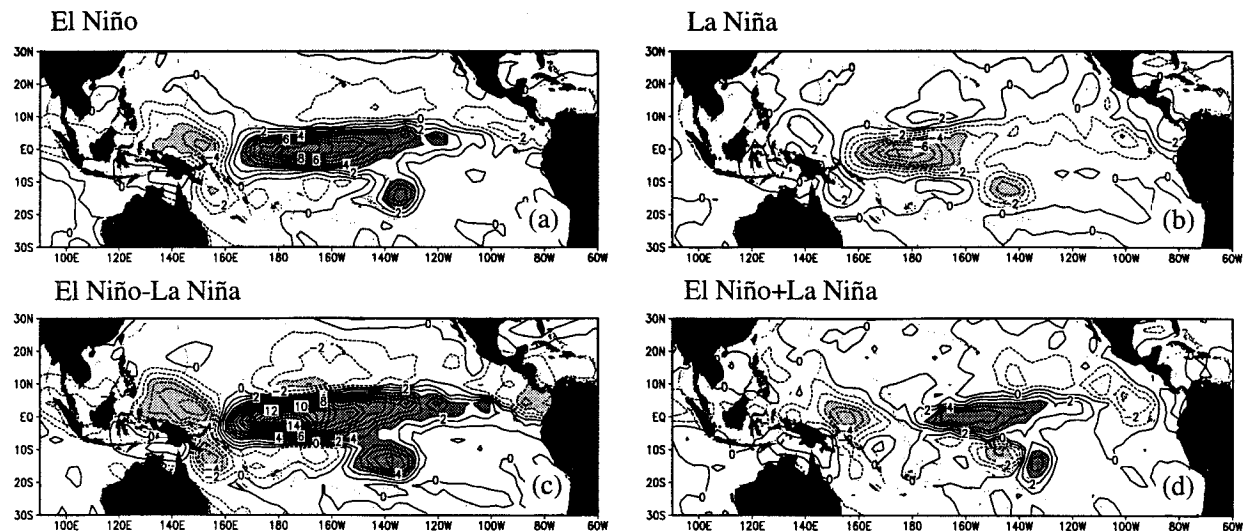
El Niño

La Niña

El Niño-La Niña

El Niño+La Niña

FIG. 8. Ensemble atmospheric general circulation model DJF rainfall response to (a) El Niño and (b) La Niña composite states of the tropical Pacific sea surface temperatures. The El Niño and La Niña sea surface temperature anomalies used in these simulations are exactly equal and opposite. (c) Linear component of the simulated rainfall response, as estimated by the difference (a) – (b). (d) Nonlinear component of the simulated rainfall response, as estimated by the sum (a) + (b). Contour interval is 1 mm day^{-1}. Positive (negative) rainfall anomalies greater (less) than 3 mm day^{-1} are shaded dark (light). Mercator projection displays the tropical Pacific region 30°N–30°S.
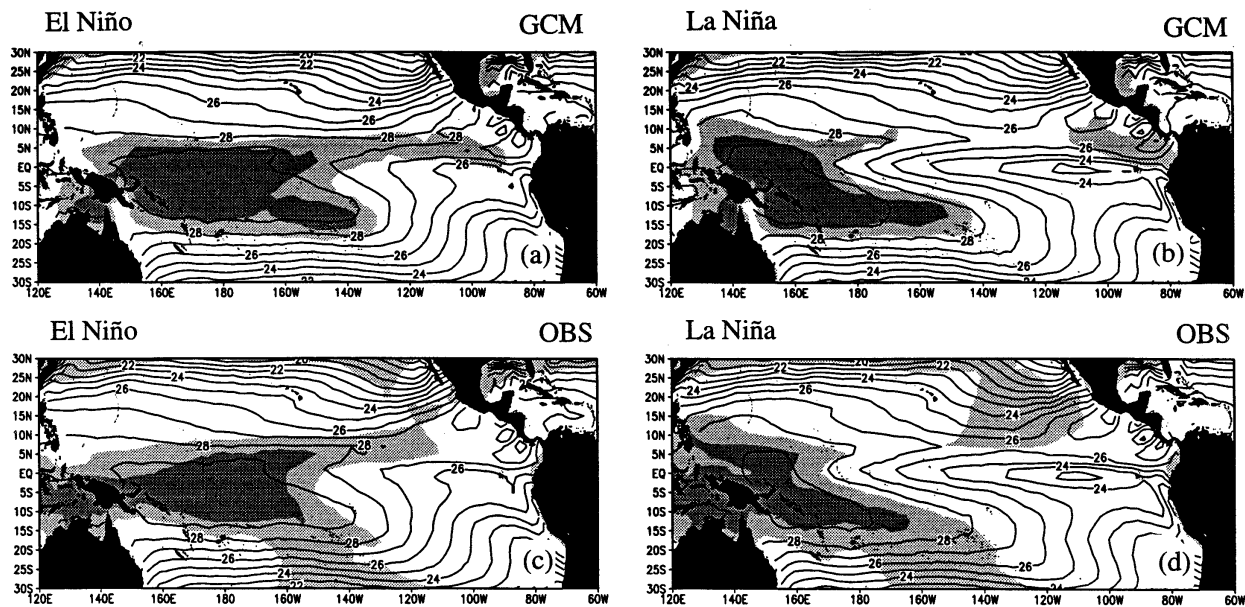
El Niño   GCM   La Niña   GCM

El Niño   OBS   La Niña   OBS

FIG. 9. Contours of the DJF total SSTs (units in °C) used as lower boundary conditions in the AGCM for (a) El Niño and (b) La Niña SST states. Overlay indicates the AGCM's simulated total rainfall (units in mm day^{-1}) for that particular SST state. The corresponding analysis of observations for (c) El Niño and (d) La Niña composite SST states. The rainfall estimates for observations are based on analysis of OLR data, as in Fig. 5. Light (dark) shading highlights rainfall rates greater than 6 (10) mm day^{-1}.

the same mechansim may be important in nature. The fact that the observed SST anomalies during El Niño are not strictly the inverse of their La Niña counterparts (see Fig. 7) may thus be of secondary importance for the local rainfall.

As mentioned earlier, preferred areas of deep convection over tropical oceans depend sensitively on the total, rather than the anomalous, SSTs. Figures 9a and 9b show the wintertime simulated total rainfall for El Niño and La Niña conditions, respectively, superimposed on the corresponding total SSTs. The rainfall covers a large zonal band of the equatorial Pacific, associated with the large expanse of uniform warm waters during El Niño and the tendency for convection to be active at SSTs greater than 27°C. In contrast, the east Pacific cold tongue is enhanced during La Niña, and equatorial SSTs of sufficient warmth to support deep convection are confined west of the date line (see also Mitchell and Wallace 1996). The corresponding analysis of observations (Figs. 9c and 9d) confirms the realism of the AGCM behavior, in particular with respect to the large controlling effect of the equatorial Pacific SSTs on rainfall distributions. One notable exception is the southern part of the South Pacific convergence zone, where the axis of observed active convection cuts across the SST gradient. This feature, which is not well simulated in the AGCM, is apparently related to transient disturbances migrating between the subtropical and midlatitude South Pacific (e.g., Kiladis et al. 1989).

Figure 10 presents the AGCM's 500-mb height responses, and these results provide evidence that the observed nonlinearity in teleconnections is real. Consistent

with observations is a phase shift between the simulated responses over the PNA region, with the centers of action during La Niña (Fig. 10b) positioned west of their El Niño counterparts (Fig. 10a). The amplitudes of the circulation anomalies are slightly larger for the warm versus the cold tropical SST states, a feature also noted in the observed height composites. An additonal feature is a stationary wave response of large amplitude over eastern Europe during La Niña, for which there is no counterpart during El Niño.

Appreciable nonlinearity exists in the simulated extratropical circulation response (Fig. 10d), although over the PNA region this is only half the amplitude of the linear component (Fig. 10c). Of particular interest is that the spatial pattern of the AGCM's nonlinear component over the PNA region resembles that observed (see Fig. 3d), and understanding the cause for the AGCM's response may shed light on the observed behavior.

The simulated nonlinearity of the stationary wave response is primarily related to a phase shift of the teleconnection patterns, analogous to the observational composites. Time–longitude sections of the AGCM 500-mb height responses (Fig. 11) reveal that the midlatitude anomaly centers during El Niño are positioned 15° longitude east of their La Niña counterparts. This is somewhat less than the phase shift between the observed composites and is consistent with the smaller amplitude of the AGCM's nonlinear component of the extratropical response.

That the AGCM's nonlinear equatorial rain response may contribute to phase shifts of its teleconnection re-
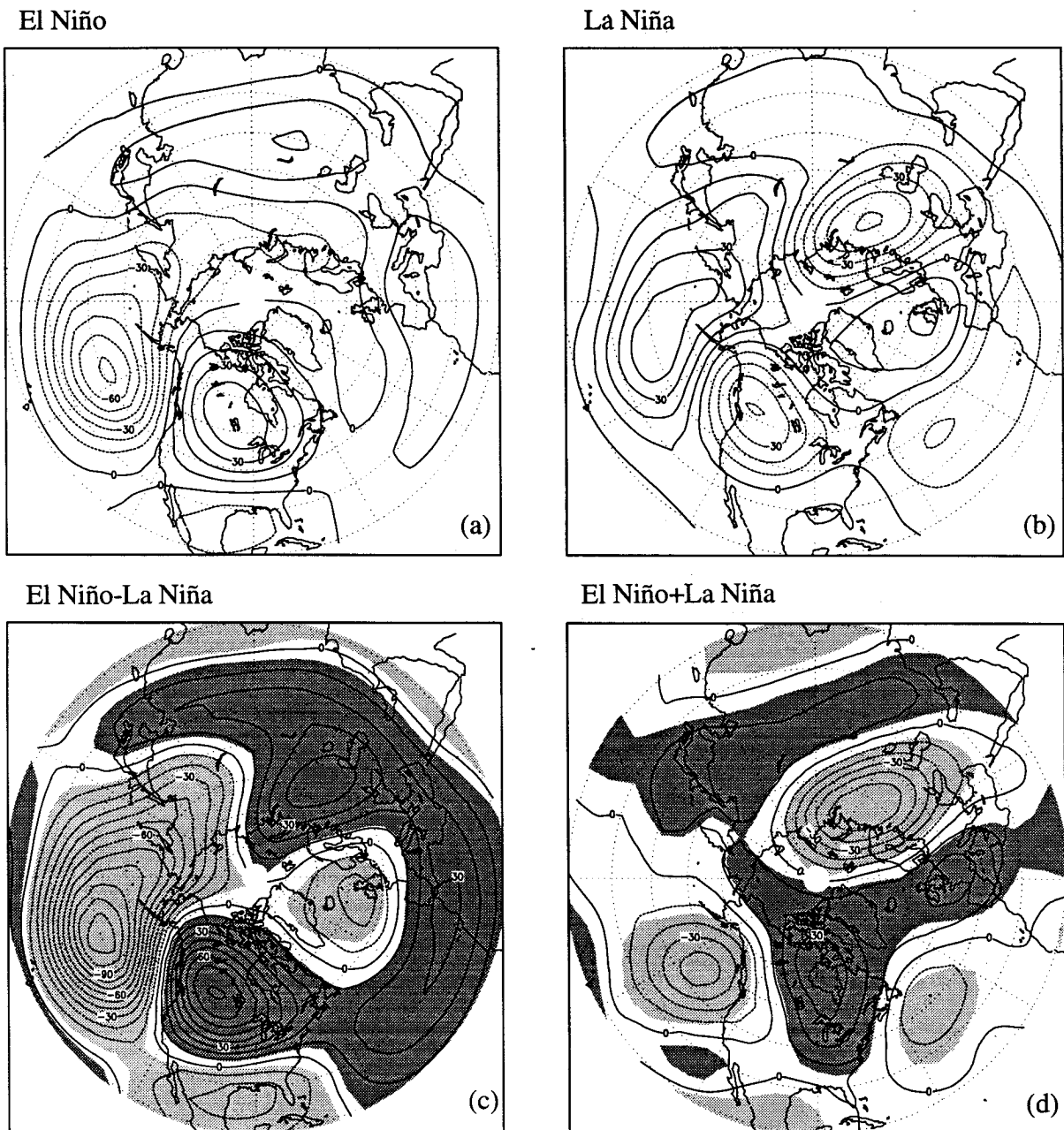
El Niño

La Niña

El Niño-La Niña

El Niño+La Niña

FIG. 10. Same as Fig. 8 except for the simulated eddy 500-mb height anomalies. Contour interval is 10 m. Dark (light) shading indicates local statistical significance of positive (negative) values at the 95% confidence level. Polar stereographic projection extends to 20°N.

sponses is suggested by the 300-mb streamfunction anomalies in Fig. 12 (note that the polar stereographic projection in these panels extends to the equator). The center of the subtropical anticyclonic response to El Niño (Fig. 12a) is located 15° longitude east of the center of the cyclonic response to La Niña (Fig. 12b). Such phase shifts are outwardly consistent with the different positions of the equatorial rain anomalies, and this relationship in the AGCM has a counterpart in the observed composites of rainfall and circulation. Such an impression can be de-

ceptive, however, and it is now well known that the subtropical circulation anomalies during El Niño (La Niña) are not a simple direct response to equatorial heating (cooling), but are also maintained by transient eddy fluxes of momentum and vorticity (e.g., Held et al. 1989; Hoerling and Ting 1994). More rigorous analysis of the AGCM data is thus in order, and the following section explores the dynamic consistency between the nonlinear components of the tropical rainfall and midlatitude stationary wave responses.
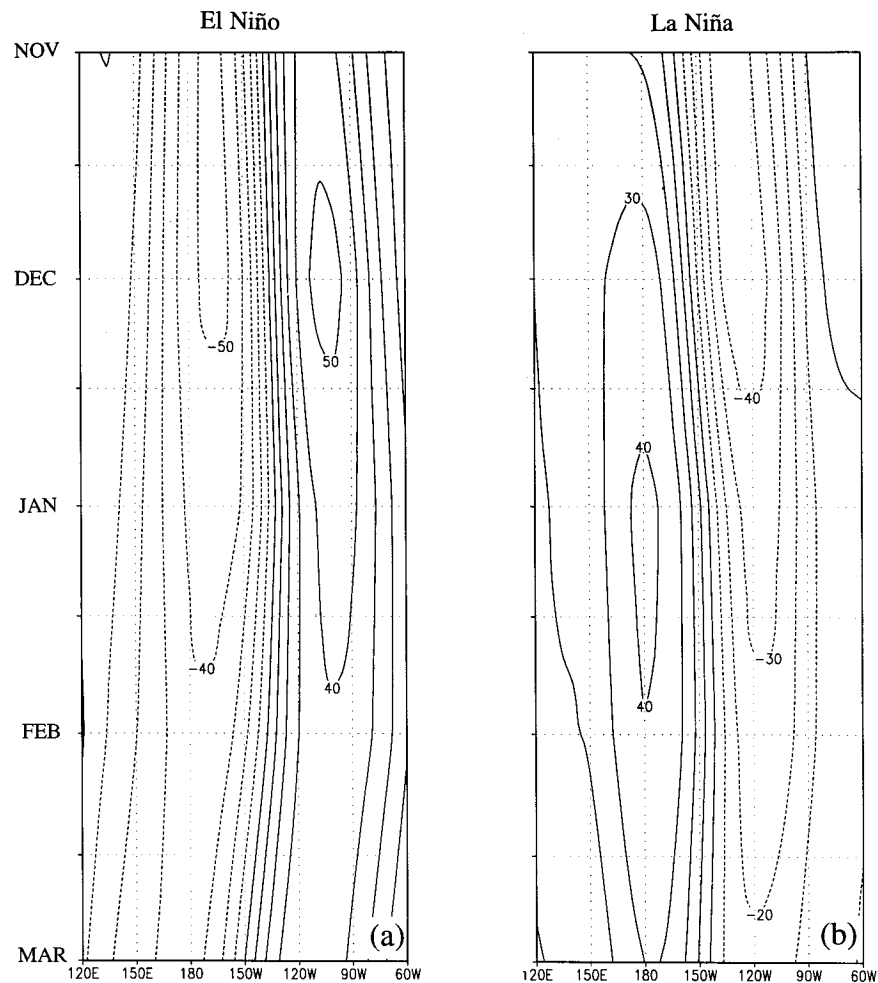
El Niño La Niña

FIG. 11. Same as Fig. 4 except for the time–longitude section for the simulated eddy 500-mb height anomalies.

5. Barotropic model analysis of the AGCM's extratropical response

Perhaps the simplest approach within a hierarchy of possible dynamical model analyses is to explore the linear response of a one-level vorticity conserving model to some proxy of the tropical convection anomalies in Fig. 8. The question thus becomes whether the tropically forced Rossby waves at a suitable approximation to the equivalent barotropic level have different phases for the forcing patterns associated with El Niño and La Niña. We specifically inquire whether the asymmetric component of the AGCM's 300-mb circulation anomalies (Fig. 12d) can be understood as the forced stationary wave response to the asymmetric component of the tropical convective anomalies (Fig. 8d).

Figure 13 shows the AGCM's divergence anomalies at the 200-mb level of maximum outflow from the tropical deep convection, and these should be compared to their respective rainfall counterparts in Fig. 8. Note especially that divergence anomalies during El Niño (Fig.

13a) and La Niña (Fig. 13b) correspond closely to the pattern of rainfall anomalies within 20° of the equator, although a more thorough analysis is needed to assess their full consistency. Divergence anomalies at higher latitudes do not appear to be directly related to local rainfall, and they are presumably indicative of the adjustment to the storm track and stationary wave anomalies (e.g., Held and Kang 1987; Held et al. 1989). Consistent with the rainfall response, the linear component of the divergence response dominates (Fig. 13c), and the weaker nonlinear component (Fig. 13d) strongly resembles the El Niño pattern itself.

Divergence anomalies for the entire tropical band within 20°N–20°S are used as input to the barotropic model, and the imposed Rossby wave forcing associated with that divergence is given by the first right side term of (2) in section 2c. Figure 14 shows the forced solutions when the barotropic model is linearized about the 300-mb wavy state that is derived from the control AGCM run using climatological SSTs. Each panel
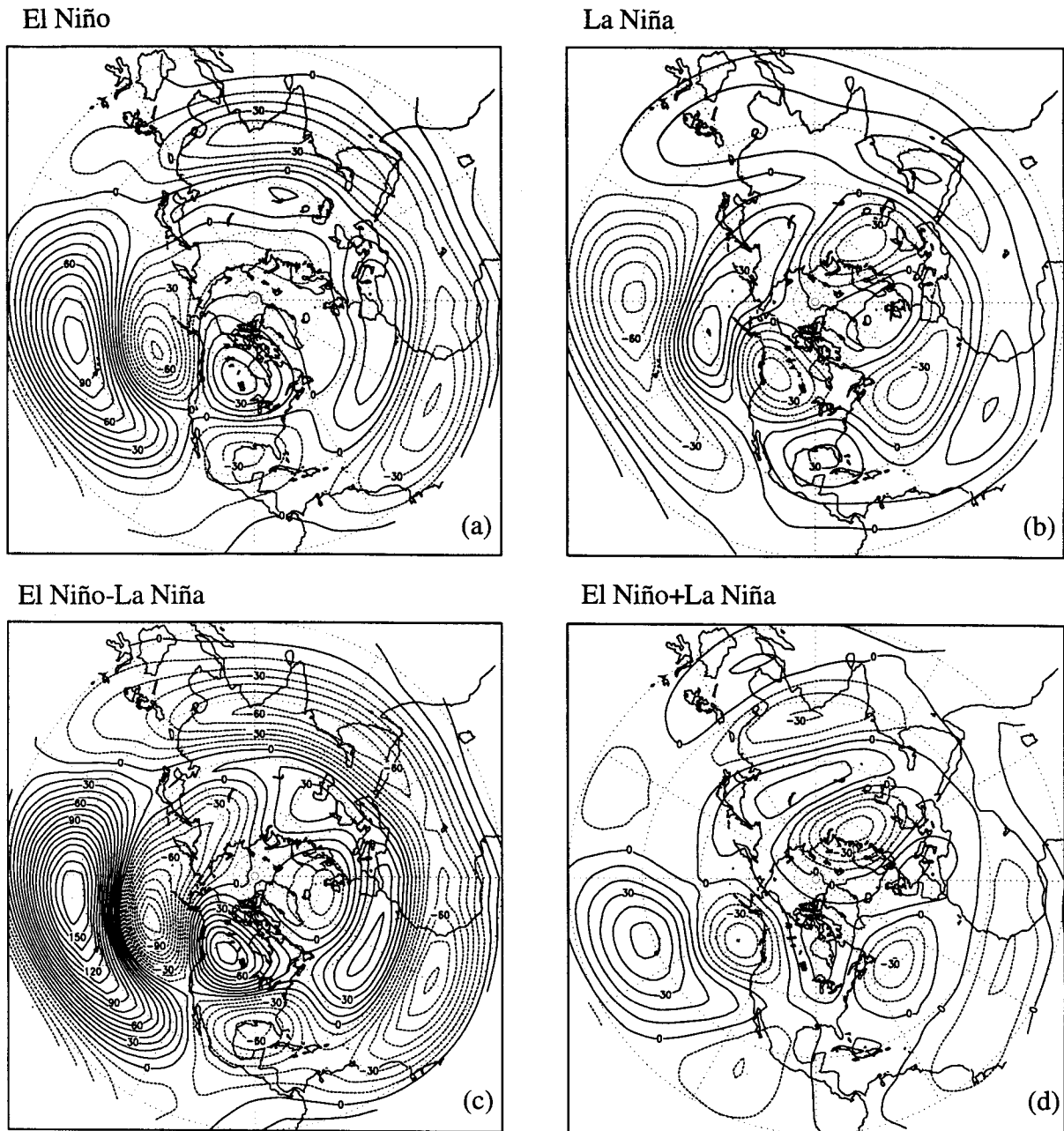
El Niño

La Niña

El Niño-La Niña

El Niño+La Niña

FIG. 12. Same as Fig. 10 except for the simulated eddy 300-mb streamfunction anomalies (units in 10^5 m^2 s^{-1}). Polar stereographic projection extends to the equator.

shows the response to the tropical divergence anomalies of the corresponding panel of Fig. 13.

The stationary wave response to the El Niño divergence anomalies (Fig. 14a) consists of a wave train, having maximum amplitude over the Pacific–North American region, that is shifted 30° longitude east of the wave train forced by the La Niña divergence anomalies (Fig. 14b). This phase shift is somewhat greater than that encountered in the AGCM, although perhaps coincidentally it is nearly identical to the observed dif-

ference in phase between warm and cold event teleconnection patterns. The key point here is that when considering the direct effect of tropical forcing alone, differences in the spatial patterns of that forcing between cold and warm events are adequate to drive different teleconnection patterns. Note further that the nonlinear component of the AGCM's 300-mb streamfunction response over the PNA region is realistically simulated when the barotropic model is forced with the nonlinear component of the tropical divergence (cf. Figs. 12d and
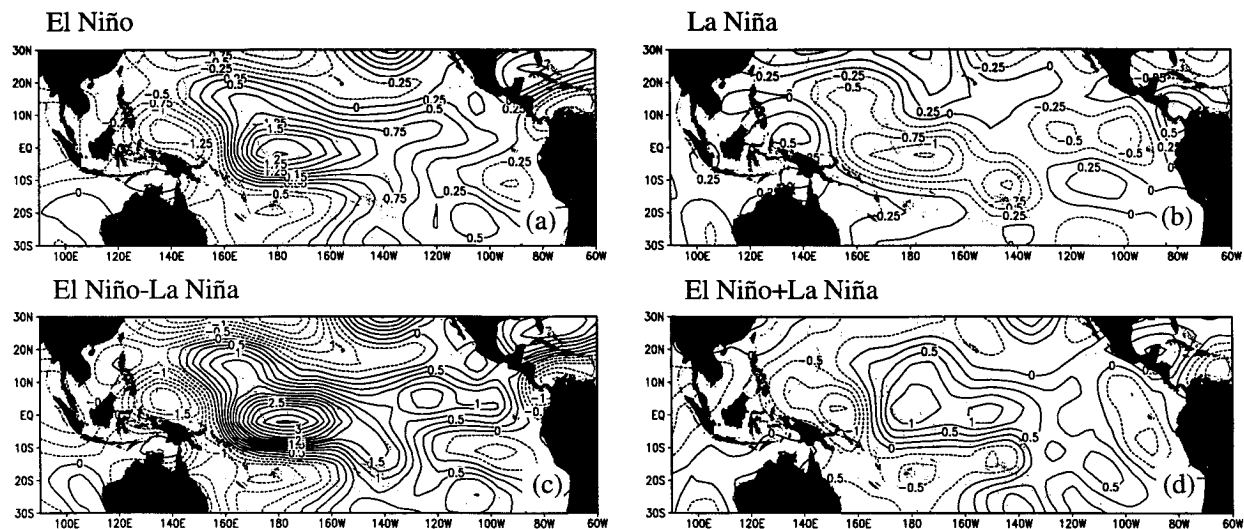
El Niño

La Niña

El Niño-La Niña

El Niño+La Niña

FIG. 13. Same as Fig. 8 except for the simulated 200-mb divergence anomalies (units in 10^{-6} s^{-1}).

14d). Although these barotropic experiments do not exclude a role for other dynamic sources of the extratropial response, they do offer evidence that the nonlinear SST–rainfall relationship of tropical latitudes alone may be important for inducing different phases of the teleconnection responses.

6. Summary and concluding remarks

This paper deals with the assessment of inherent nonlinearities in the atmospheric system to equal and opposite tropical Pacific SST forcing. The study inquires in particular whether such behavior may be a plausible explanation for the emerging evidence that the Northern Hemispheric climate does not vary in a linear manner with respect to extremes in the El Niño–Southern Oscillation. This additional signal associated with departures from linearity is nonetheless smaller than the observed circulation variability from one ENSO winter to another that results mainly from the chaotic behavior of the flow itself (Kumar and Hoerling 1997).

Our observational analysis for the 1950–96 period suggests that the North American surface temperature anomalies during El Niño exhibit a near-quadrature relation with their La Niña counterparts, and these deviate significantly from two inverse states with respect to the SO. Likewise, circulation anomalies in the upper troposphere also exhibit appreciable nonlinearity. Similar evidence that the atmospheric system varies nonlinearly to opposite phases of the Southern Oscillation has also emerged from other observational studies using compositing techniques (e.g., Dole et al. 1994; Sittel 1994; Montroy et al. 1996, manuscript submitted to *J. Climate*; Livezey et al. 1997).

A notable feature of the circulation anomalies in the upper troposphere during northern winter is a phase shift in the teleconnection patterns over the Pacific–North

American region between El Niño and La Niña composites, and there is an indication that the two wave trains have different tropical source regions. Indeed, analysis of OLR data suggests that maximum positive rainfall anomalies are located east of the date line during El Niño, but slightly west of the date line during La Niña. Such behavior is consistent with the well-known sensitivity of deep convection to the total, rather than the anomalous, value of sea surface temperature.

Due to several caveats, observations alone offer insufficient evidence for an inherently nonlinear atmospheric sensitivity to tropical SST forcing. The brevity of the observational record implies that compositing cannot serve to eliminate all circulation features unrelated to the SST forcing, and results based on such methods yield some blend of climate signal and climate noise. The fact that the composite SST anomalies for warm and cold phases of the SO are also not equal and opposite further confounds interpretation of the atmospheric behavior.

A suite of idealized atmospheric GCM experiments was thus performed in order to determine the climate system's inherent sensitivity to precisely equal and opposite phases of tropical Pacific SST forcing typically encountered during ENSO. Although idealized in their construct of linearity, the SST anomalies evolve through realistic, seasonally varying life cycles possessing amplitudes and spatial scales typically seen during a basinwide event. A 40-member ensemble of such simulations, performed separately for warm and cold SST states, was found to exhibit a nonlinear climate response that in many ways resembled the observations. First, the AGCM's equatorial Pacific rain response was maximized east of the date line during El Niño, but west of the date line during La Niña. This difference, associated with an inherently nonlinear SST–rain relationship in the Tropics, was accompanied by a simulated telecon-

El Niño

La Niña

(a)

(b)

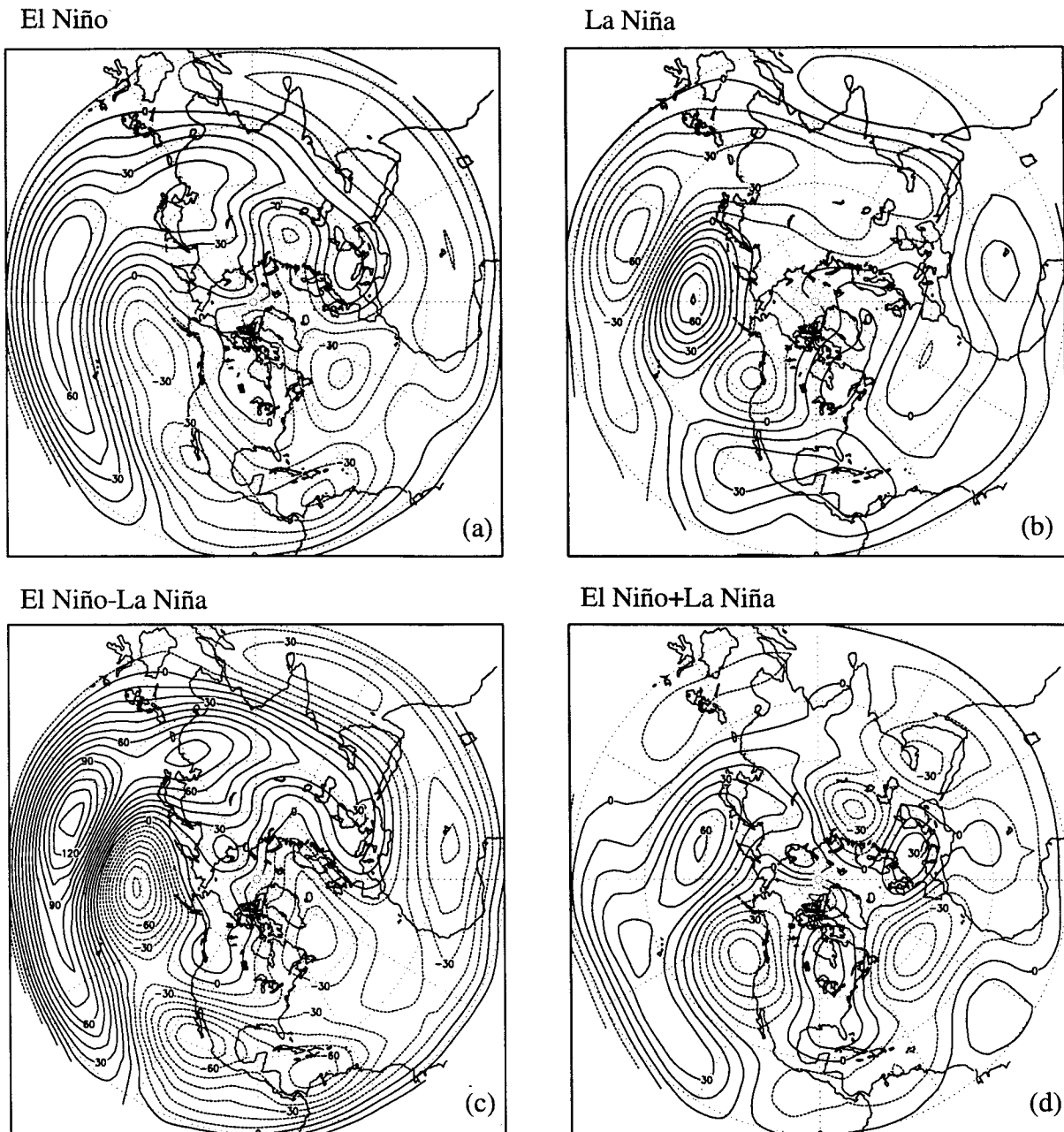El Niño-La Niña

El Niño+La Niña

(c)

(d)

FIG. 14. Eddy streamfunction anomalies at 300 mb for the barotropic model response linearized about the AGCM's zonally varying climatology and subjected to the AGCM's 20°N–20°S tropical divergence anomalies related to (a) El Niño, (b) La Niña, (c) the difference of El Niño minus La Niña divergence anomalies, and (d) the sum of El Niño plus La Niña divergence anomalies. Contour interval and map projection are as in Fig. 12.

nection response over the PNA region, phase shifted 15° longitude east during El Niño relative to La Niña. Although more modest than the phase shift noted in observations, it once again suggested the existence of different tropical source regions for the upper-tropospheric wavetrains.

A question of considerable scientific interest is whether the differences in extratropical responses are primarily due to differences in the tropical heating, or whether additional dynamic sources also play an important role (e.g., changes in the mean flow through which the energy from tropical sources propagates, or sensitivity of the storm track feedbacks). Thus, a more rigorous assessment of the dynamic significance of differences in tropical convective responses to warm and cold SSTs was conducted using a one-level vorticity conserving model. This model was linearized about the AGCM zonally varying upper-tropospheric climatolog-

ical flow and forced separately with the tropical divergence anomalies associated with the warm and cold event simulations. Appreciable sensitivity to the differences in forcing was found. The Rossby waves forced by warm event divergence anomalies were found to follow ray paths 30° longitude east of those forced by the AGCM's cold event divergence anomalies. The phase shift between the AGCM's teleconnection responses to warm and cold tropical Pacific SSTs was thus argued to originate at least in part from the nonlinear SST–rainfall relationship, which leads to different patterns of Rossby wave forcing, despite equal and opposite SST forcing.

Other sources for nonlinearity, including changes in the basic-state flow associated with the direct response to heating and sensitivity of transient eddy interactions, remain to be explored. With regard to the former, several additional calculations were performed to assess whether forced solutions of the barotropic model were sensitive to different basic states. Results from the barotropic experiments were found not to depend on whether the model was linearized about the zonally varying flow of the El Niño or La Niña states themselves (not shown). The propagation characteristics of the forced Rossby waves were thus not sensitive to the modest flow anomalies associated with El Niño or La Niña SST anomalies. Such a lack of sensitivity implies that changes in the mean flow induced by tropical heating may not be of further importance in generating an asymmetric teleconnection response.

Judgement of the possible significance of a nonlinear component of the climate system's response to ENSO, relative to the linear component in particular, must await further analyses with different GCMs or dynamical models. It is, on one hand, encouraging that the particular general circulation model used herein was able to simulate with high fidelity the linear and nonlinear components of the tropical rainfall responses to the SST forcing. The further complications involved in tropical–extratropical interactions, however, mean that equal fidelity is not guarenteed for the simulated teleconnection responses. To be sure, these were shown to be realistic for El Niño and La Niña SST states, but the fact remains that the implied nonlinearity of teleconnections seen in observations is much larger than simulated in our controlled experiments. It should be noted in this regard that given the importance of an SST–rainfall nonlinearity, the selection of SST patterns different in amplitude and distribution from those considered herein is also warranted. Nonlinearity of the atmospheric response may also be a sensitive function of the annual cycle, given the strong annual cycle of climatological SST in the equatorial east Pacific.

Thus, although our analysis confirms a physical basis for nonlinearity, the question remains open as to its significance. We would argue that some benefit can accrue in seasonal prediction efforts that distinguish between the climate signals of extremes in the Southern Oscillation, although it remains to be determined whether gains in skill will be as large as implied by Fig. 1.

REFERENCES

Arkin, P. A., and B. N. Meisner, 1987: The relationship between large-scale convective rainfall and cold cloud over the Western Hemisphere during 1982–84. *Mon. Wea. Rev.,* **115,** 51–74.

Barnston, A., and R. E. Livezey, 1987: Classification, seasonality, and persistence of low-frequency circulation patterns. *Mon. Wea. Rev.,* **115,** 1083–1126.

Blade, I., and D. L. Hartmann, 1995: The linear and nonlinear extratropical response of the atmosphere to tropical intraseasonal heating. *J. Atmos. Sci.,* **52,** 4448–4471.

Borges, M. D., and P. D. Sardeshmukh, 1995: Barotropic Rossby wave dynamics of zonally varying upper-level flows during northern winter. *J. Atmos. Sci.,* **52,** 3779–3796.

Bradley, R. S., H. F. Diaz, G. N. Kiladis, and J. K. Eischeid, 1987: ENSO signal in continental temperature and precipitation records. *Nature,* **327,** 497–501.

Branstator, G., 1995: Organization of storm track anomalies by recurring low-frequency circulation anomalies. *J. Atmos. Sci.,* **52,** 207–226.

Deser, C., and J. M. Wallace, 1990: Large-scale atmospheric circulation features of warm and cold episodes in the tropical Pacific. *J. Climate,* **3,** 1254–1281.

Dole, R. M., K. Paine, and K. E. Wolter, 1994: Short-term climate extremes over the continental U.S. and ENSO. *Proc. 19th Annual Climate Diagnostics Workshop,* College Park, MD, NOAA/NCEP/Climate Prediction Center, 18–20.

Gadgil, S., P. V. Joseph, and N. V. Joshi, 1984: Ocean–atmosphere coupling over monsoon regions. *Nature,* **312,** 141–143.

Held, I. M., and I.-S. Kang, 1987: Barotropic models of the extratropical responses to El Niño. *J. Atmos. Sci.,* **44,** 3576–3586.

——, S. W. Lyons, and S. Nigam, 1989: Transients and the extratropical response to El Niño. *J. Atmos. Sci.,* **46,** 163–174.

Hoerling, M. P., and M. Ting, 1994: Organization of extratropical transients during El Niño. *J. Climate,* **7,** 745–766.

——, M. L. Blackmon, and M. Ting, 1992: Simulating the atmospheric response to the 1985–87 El Niño cycle. *J. Climate,* **5,** 665–682.

——, L. Sanford, and J. Hurrell, 1993: Diagnosis and sensitivity of the wintertime 200mb circulation in NCAR CCMs. NCAR Tech. Rep. NCAR/TN-394+STR, 68 pp. [Available from NCAR, P.O. Box 3000, Boulder, CO 80307.]

Kiladis, G. N., and H. F. Diaz, 1989: Global climatic anomalies associated with extremes in the Southern Oscillation. *J. Climate,* **2,** 1069–1090.

——, H. von Storch, and H. van Loon, 1989: Origins of the South Pacific convergence zone. *J. Climate,* **2,** 1185–1195.

Kumar, A., and M. P. Hoerling, 1997: Interpretation and implications of observed inter–El Niño variability. *J. Climate,* **10,** 83–91.

——, ——, M. Ji, A. Leetmaa, and P. D. Sardeshmukh, 1996: Assessing a GCM's suitability for making seasonal predictions. *J. Climate,* **9,** 115–129.

Liebmann, B., and C. A. Smith, 1996: Description of a complete

(interpolated) outgoing longwave radiation dataset. *Bull. Amer. Meteor. Soc.,* **77,** 1275–1277.

Livezey, R. E., A. Leetmaa, M. Mautani, H. Rui, N. Ji, and A. Kumar, 1997: Teleconnective response of the Pacific–North American region atmosphere to large central equatorial Pacific SST anomalies. *J. Climate,* **10,** 1787–1820.

Mitchell, T. P., and J. M. Wallace, 1996: ENSO seasonality: 1950–78 versus 1979–92. *J. Climate,* **9,** 3149–3161.

Pan, Y.-H., and A. H. Oort, 1983: Global climate variations connected with sea surface temperature anomalies in the eastern equatorial Pacific Ocean for the 1958–73 period. *Mon. Wea. Rev.,* **111,** 1244–1258.

Philander, S. G., 1990: *El Niño, La Niña, and the Southern Oscillation.* Academic Press, 293 pp.

Rasmusson, E. M., and T. H. Carpenter, 1982: Variations in sea surface temperature and surface wind fields associated with the Southern Oscillation/El Niño. *Mon. Wea. Rev.,* **110,** 354–384.

Reynolds, R. W., and T. A. Smith, 1994: Improved global sea surface temperature analysis using optimum interpolation. *J. Climate,* **7,** 929–948.

Ropelewski, C. F., and M. S. Halpert, 1989: Precipitation patterns associated with the high index phase of the Southern Oscillation. *J. Climate,* **2,** 268–284.

Sardeshmukh, P. D., and B. J. Hoskins, 1988: The generation of global rotational flow by steady idealized tropical divergence. *J. Atmos. Sci.,* **45,** 1228–1251.

Sittel, M. C., 1994: Marginal probabilities of the extremes of ENSO for temperature and precipitation in the southeastern United States. FSU Tech. Rep. 94-1. [Available from Center for Ocean–Atmospheric Studies, 020 Love Building, The Florida State University, Tallahassee, FL 32306-3041.]

Smith, T. M., R. W. Reynolds, R. E. Livezy, and D. Stokes, 1996: Reconstruction of historical sea surface temperatures using empirical orthogonal functions. *J. Climate,* **9,** 1403–1420.

Ting, M., 1996: Steady linear response to tropical heating and barotropic in baroclinic models. *J. Atmos. Sci,* **53,** 1698–1709.

——, and I. M. Held, 1990: The stationary wave response to a tropical SST anomaly in an idealized GCM. *J. Atmos. Sci.,* **47,** 2546–2566.

Trenberth, K. E., and D. A. Paolino, 1980: The Northern Hemisphere sea level pressure dataset: Trends, errors, and discontinuities. *Mon. Wea. Rev.,* **108,** 855–872.

van Loon, H., and J. C. Rogers, 1981: The Southern Oscillation. Part II: Associations with changes in the middle troposphere in the northern winter. *Mon. Wea. Rev.,* **109,** 1163–1168.